Nano Energy 32 (2017) 302–309

Contents lists available at ScienceDirect

Nano Energy

journal homepage: www.elsevier.com/locate/nanoen

Full paper

In situ atomic-scale observation of reversible sodium ions migration in layered metal dichalcogenide SnS_2 nanostructures

Peng Gao[a,b,*], Yu-Yang Zhang[c], Liping Wang[d], Shulin Chen[a], Yuan Huang[e], Xiumei Ma[a], Kaihui Liu[b,f], Dapeng Yu[b,f]

[a] *Electron Microscopy Laboratory, School of Physics, Peking University, Beijing 100871, China*
[b] *Collaborative Innovation Center of Quantum Matter, Peking University, Beijing 100871, China*
[c] *School of Physical Sciences and CAS Key Laboratory of Vacuum Physics, University of Chinese Academy of Sciences, Beijing 10049, China*
[d] *State Key Laboratory of Electronic Thin Films and Integrated Devices, University of Electronic Science and Technology of China, Chengdu 610054, China*
[e] *Center for Functional Nanomaterials, Brookhaven National Laboratory, Upton, NY 11973, United States*
[f] *State Key Laboratory for Mesoscopic Physics, School of Physics, Peking University, Beijing 100871, China*

ARTICLE INFO

Keywords:
Sodium ion battery
In situ TEM
Structure ordering
Ion migration
Layered metal dichalcogenide

ABSTRACT

Ion migration in solids provides basis for a wide range of technique applications including alkali-metal ion batteries. Understanding the ion migration dynamics and kinetics is critical to bring benefits to the industry. Here, we directly track the Na ions insertion and extraction in van der Waals interactions dominated layered structure SnS_2 at atomic-scale by *in situ* transmission electron microscopy technique. Insertion of sodium in SnS_2 forms highly defective and expanded Na_xSnS_2 with volume expansion of (~5%) via a two-phase reaction while sodium extraction involves a solid solution behavior with formation of nano-sized intermediate superstructure $Na_{0.5}SnS_2$, of which the atomic structure has been identified to be row ordering in the (001) planes. The reaction behaviors of sodiation are also compared with lithiation in SnS_2 nanostructures. Unlike the conversion and ionic bonded intercalation-type electrode materials, in this van der Waals material SnS_2 the sodiation and lithiation reactions share great similarities in the dynamics (e.g. asymmetric reaction pathways). However, the high density of defects that are generated at the reaction front during sodiation, was not captured during lithiation probably due to the larger radius and heavy mass for Na ions. These findings provide valuable insights into understanding the underlying ion migration mechanism in the layered transition metal dichalcogenide. The asymmetric sodium insertion and extraction pathways may help us to elucidate the origins of voltage hysteresis and energy efficiency in alkali-metal ion batteries.

1. Introduction

Recently, the sodium ion batteries (SIBs) [1–3] have attracted a lot of research interest for the emerging large-scale applications of electric vehicles and grid storage [4,5] because of the concerns about the limited natural abundance and uneven global distribution of lithium. Finding suitable electrode materials (both cathodes and anodes) for SIBs, however, remains challenging as many electrode materials that function well in the lithium ion batteries (LIBs) are no longer suitable for SIBs. For example, few sodium ions can be intercalated in the graphite (NaC_{70} in ref. [6]), although it is the most commonly used anode in LIBs (LiC_6) [6]. Previously, it is widely accepted that the sodium ions having a larger radius and heavier mass compared to lithium ions account for the low capacity in the Na-graphite system. The recent calculations suggested the low sodium capacity originates from the weak chemical bonding between sodium and graphite [7]. Such mechanism may also applies to other electrode materials for sodium batteries [7].

Nevertheless, it is reported recently that the layered metal dichalcogenides such as MoS_2 and SnS_2 also have a similar layered structure with graphite but can effectively accommodate Na, enabling them to be alternatives as electrode materials for high capacity SIBs [8–11]. However, the behaviors of alkali ions migration in these van der Waals interactions dominated layered metal dichalcogenide structures [12–15] could be very different than those in the covalent or ionic transition metal oxides with variable valences, which adopt lithium ions by only adjusting the valence of transition metal ions but the entire crystal structure framework remains almost unchanged. In contrast, for the layered metal dichalcogenides bonded by the weak van der Waals interaction, the intercalated alkali ions can significantly modify

* Corresponding author at: Electron Microscopy Laboratory, School of Physics, Peking University, Beijing 100871, China.
E-mail address: p-gao@pku.edu.cn (P. Gao).

http://dx.doi.org/10.1016/j.nanoen.2016.12.051
Received 24 October 2016; Received in revised form 16 December 2016; Accepted 26 December 2016
Available online 27 December 2016

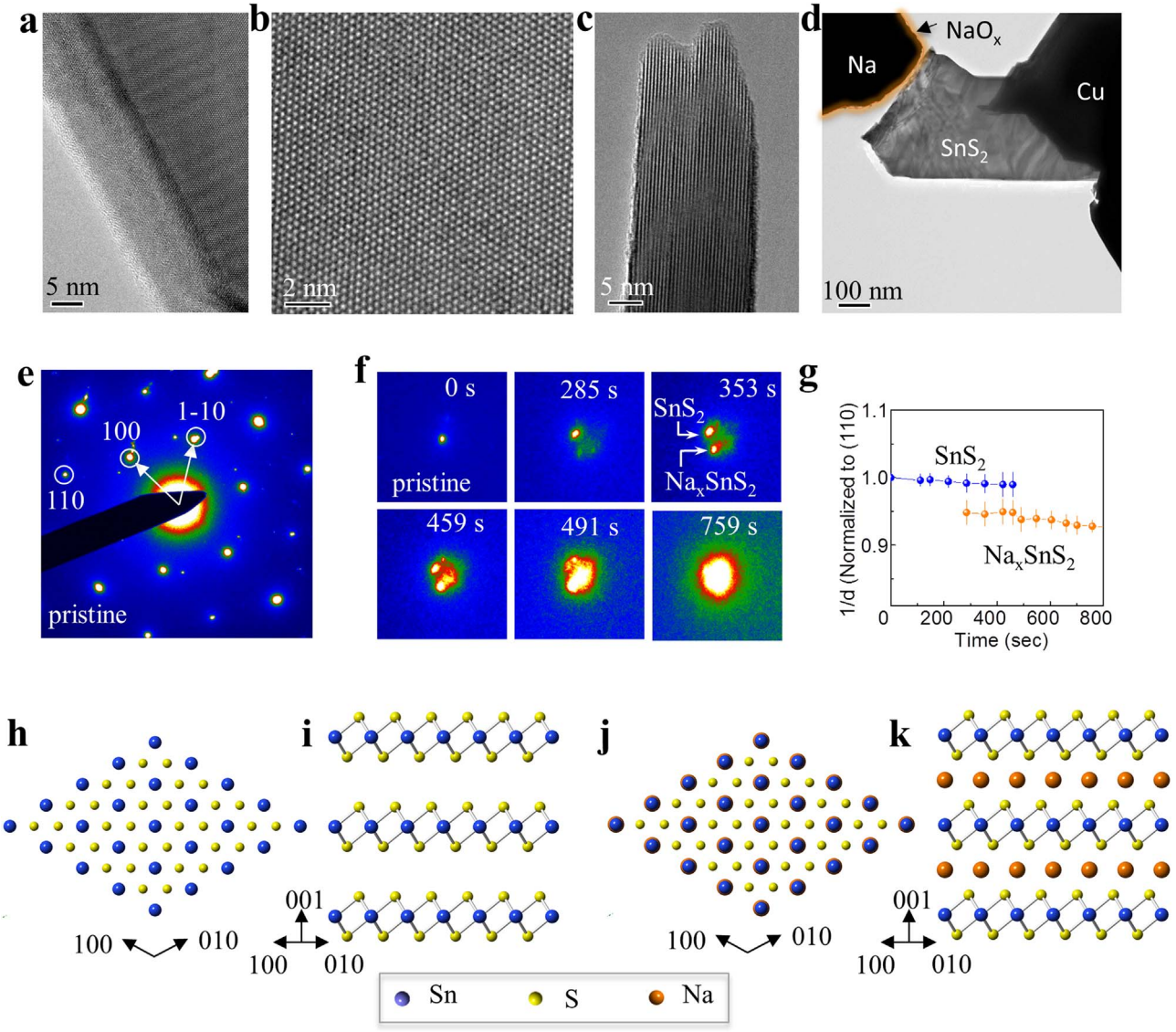

Fig. 1. Real-time tracking Na ions transport in SnS_2 nanostructures. (a) A TEM image of SnS_2nanosheet. (b) A high resolution TEM image with viewing direction of [001]. (c) A high resolution TEM image with viewing direction perpendicular to [001]. (d) A TEM image shows a Na-SnS_2 battery cell used for *in situ* TEM measurements. SnS_2 nanosheet with thickness in a few nanometers were peeled off from the single crystal SnS_2. A solid battery cell consists of a very thin sheet of SnS_2 and Na counter electrode. (e) Selected area electron diffraction pattern of a pristine SnS_2nanosheet. (f) Evolution of the electron diffraction spot of (110)-SnS_2 during sodium insertion in SnS_2. (g) The sodium insertion induced lattice expansion is measured from the electron diffraction spot of (110)-SnS_2. Blue: pristine phase. Orange: sodium intercalated phase. An atomistic structure of the SnS_2 with viewing directions of (h) [001] and (i) [100]. An atomistic structure of the $NaSnS_2$ with viewing directions of (j) [001] and (k) [100].

the interactions between the layers and thus may alter the host structure. For example, Li migration in MoS_2 could cause a phase transformation from 2H to 1T [16]. Localized structural ordered staging phases (where the Li segregates between alternating (001) planes) was reported in TiS_2 during Li insertion [17] because the formation of such staging phase can effectively reduce the repulsive interaction between alkali ions [17]. Nevertheless, experimentally, the dynamics and kinetics of sodium transport in these layered structures bonded by weak van der Waals interactions have been largely unknown [18] and thus motivate this study of real-time tracking the structural evolution during Na ions migration in the SnS_2 nanostructures [11].

The *in situ* techniques are ideal to monitor the ion migration in the electrode materials. The common *in situ* techniques include *in situ* X-ray diffraction [19], absorption spectroscopy [20], nuclear magnetic resonance [12,13] , and transmission electron microscopy (TEM) techniques [16,18,21–26]. Among of them, the *in situ* TEM allows us to track the alkali ions migration in the electrode materials at both a high spatial resolution (atomic scale) and high temporal resolution (sub-second) [16,18,21–26], providing unprecedented opportunities to probe the evolutions of localized structure and intermediate phases during ion migration in electrodes.

In this work, by using such *in situ* TEM method, we find that sodium ions insertion in SnS_2 occurs via two-phase reaction to form expanded (~5%) and defective Na_xSnS_2 (x~1), while sodium extraction involves intermediate nano-sized $Na_{0.5}SnS_2$ domains with local structure ordering, being solid-solution-like reaction. The sodium diffusivity is estimated at the level of 10^{-11}–10^{-10} cm^2/s, suggesting the high rate capabilities of SIBs with proper engineering. The atomic structure of the intermediate phase $Na_{0.5}SnS_2$ is proposed based on the high resolution TEM images. The $Na_{0.5}SnS_2$ phase has alternative Na and vacancies rows along [110] direction within every (001) Na plane, which is distinct from the common staging phase that consists of Na and vacancy (001) planes. A comparison between sodiation and lithiation shows that the dynamic behaviors in such van der Waals material SnS_2 share great similarities (e.g. asymmetric reaction pathways), which is very different from the conversion electrode materials

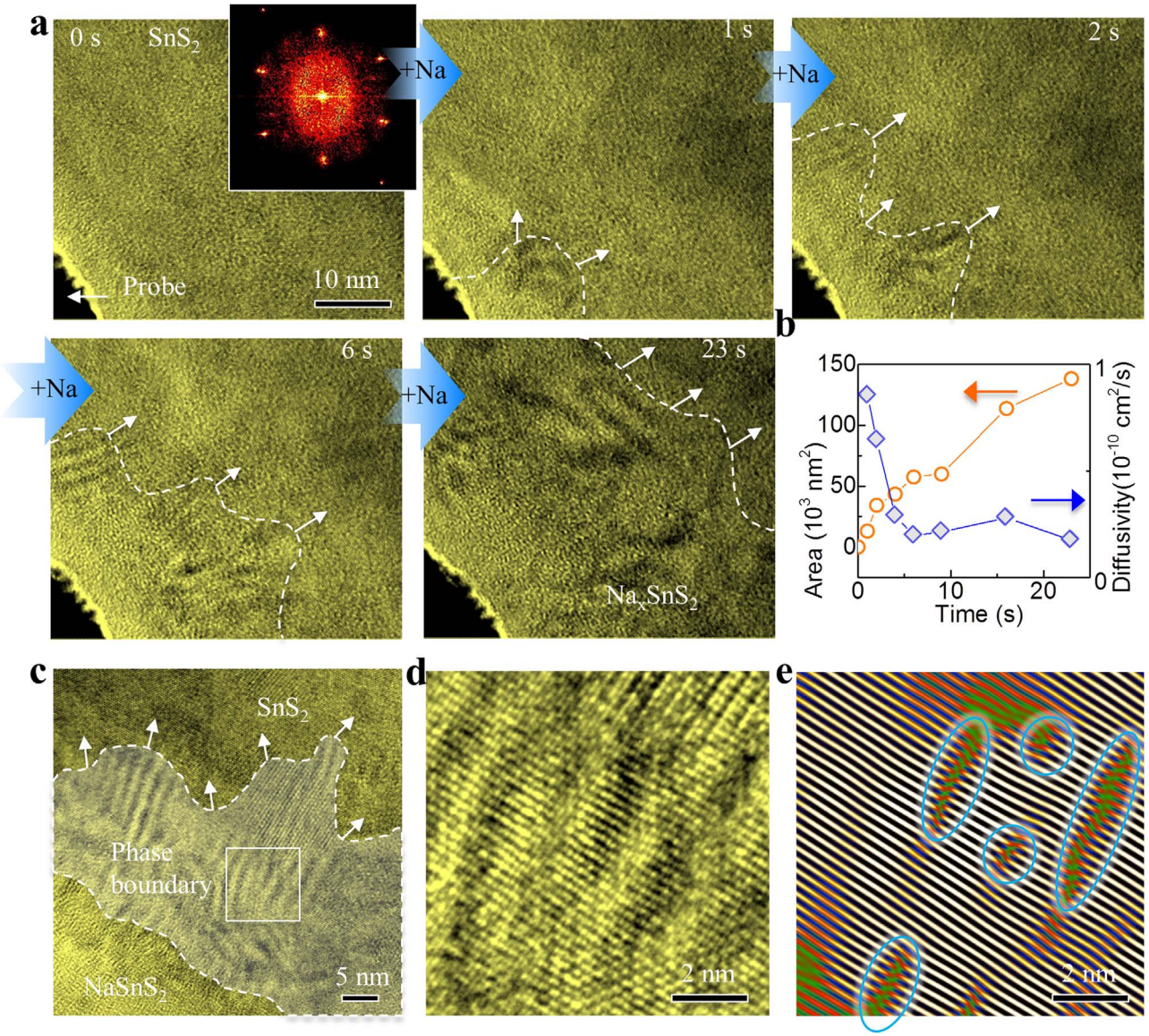

Fig. 2. High-resolution TEM tracking sodium insertion in SnS_2 in real-time. (a) Selected high-resolution TEM image series showing the propagation of the reaction front, i.e., phase boundary of $NaSnS_2/SnS_2$. Inset: FFT pattern of the pristine state indicating the viewing direction is [001]. At 1s, the sodium intercalation results in the nucleation of irregular wrinkles at the bottom-left corner. The dashed white lines roughly highlighting the reaction front for eye guidance. The white thin arrows showing the propagation direction of reaction front. (b) Area of the sodium intercalated domain and the estimated diffusivity (change in domain area with time) are plotted as a function of time. Orange: sodium intercalated domain area. Blue: estimated diffusivity (change in the domain area). (c) An enlarged view of the phase boundary. (d) TEM image and (e) the corresponding FFT filtered image of the selected region by only including the (*h00*) frequencies. Dislocations and defects with lattice distortion are denoted by blue outlines.

or other intercalation electrode materials bonded by ionic intercalations, suggesting the van der Waals materials could be promising electrode candidates for the sodium ion batteries. Our observations provide valuable insights into the mechanistic understanding of ion migration induced solid-state phase transformations and the underlying electrochemistry in the layered structures bonded by the van der Waals interactions. The asymmetric sodium insertion and extraction pathways may shed light on the origins of voltage hysteresis in layered metal dichalcogenide electrode.

2. Results and discussion

The electrochemical measurements of coin cells consisting of Na and SnS_2 nanostructures were carried out and shown in Fig. S1, which is in good agreement with previous study [11]. In Fig. 1a–d, SnS_2nanosheet peeled from a single crystal is a few nanometers in thickness. A solid battery cell built in the TEM consists of Na, SnS_2, and a passivation layer NaO_x acting as solid-state electrolyte, as shown in Fig. 1d. The selected area electron diffraction (SAED) pattern in Fig. 1e is recorded from a pristine SnS_2nanosheet with viewing direction of [001]. Upon sodium intercalation, the time resolved SAED patterns in Fig. 1f show split of the diffraction spot {110} (see Fig. S2), which is well known to be a characteristic of two-phase reaction. Such two-phase reaction mode has also been observed during Na transport in another layered metal dichalcogenide MoS_2 from *in situ* XRD measurements [19]. The split of (110) refection between pristine and intercalated phase is measured to be ~5% in Fig. 1g, which originates from the sodium intercalation induced lattice expansion.

Although we can not directly determine the Na concentration from the electron diffraction patterns, the previous first principle calculation showed that the octahedral sites between two sulfide layers have the lowest energy for lithium intercalation [27]. Therefore, during ion intercalation all the alkali ions likely prefer to occupy all the S-octahedral sites before taking the tetrahedral sites to form $LiSnS_2$

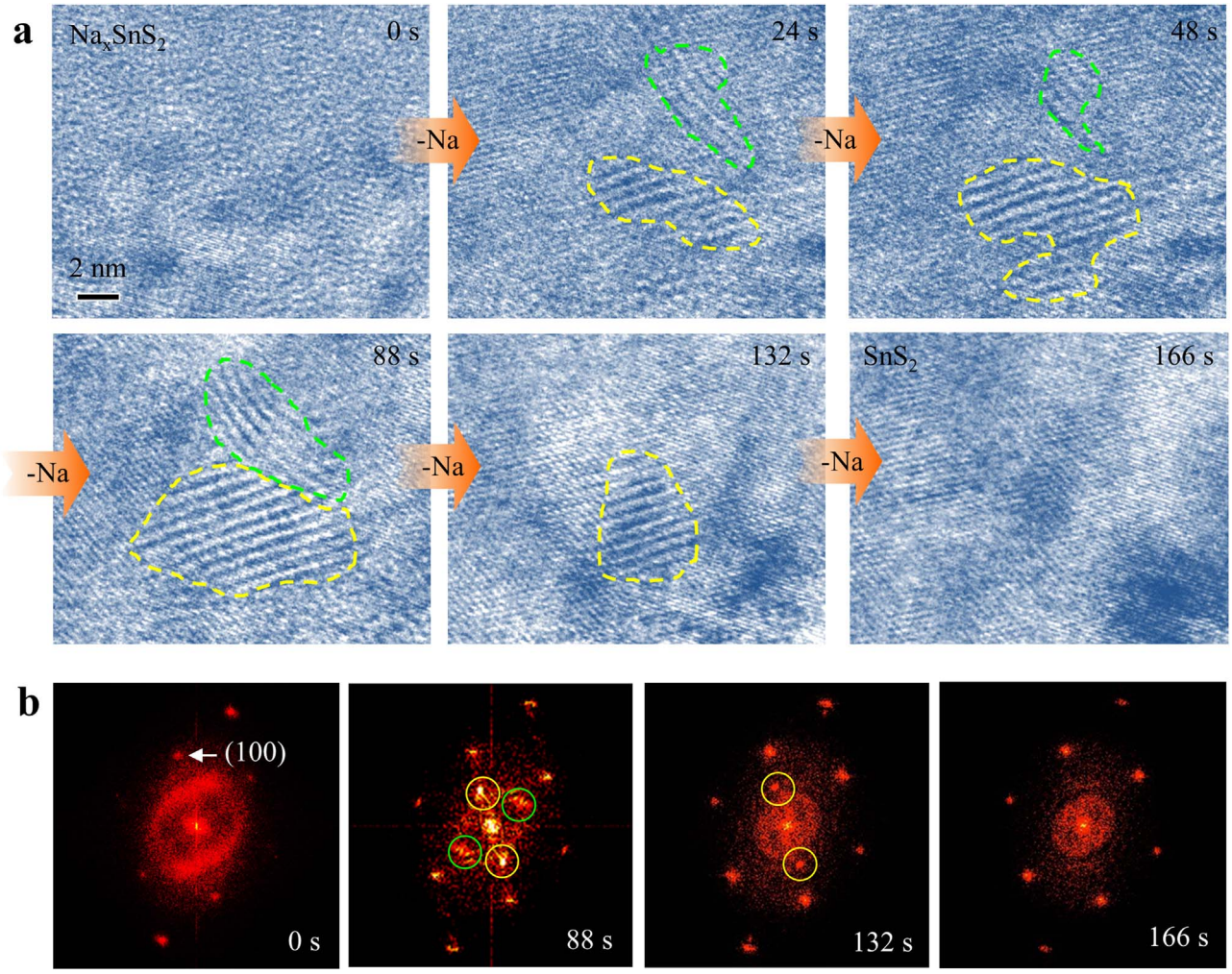

Fig. 3. High-resolution TEM tracking sodium extraction from SnS_2 in real-time. (a) Selected high-resolution TEM image series showing structural evolution during sodium extraction. The yellow and green outlines denoting the superstructured domains. (b) The corresponding FFT patterns. The reflections from superstructured domains are highlighted by the yellow and green rings. Note these stripes are not Moiré fringes because the overlapping of pristine and reacted phases caused Moiré fringes should have a space ~20 times of lattice fringes for ~5% lattice expansion.

and $NaSnS_2$. The atomic illustrations for SnS_2 and $NaSnS_2$ are shown in Fig. 1h–k.

The high-resolution TEM image series were recorded to reveal the local structural evolutions during sodium intercalation in SnS_2. Fast Fourier transform (FFT) pattern of pristine SnS_2 in Fig. 2a indicates the viewing direction is [001]. At 1s, sodium intercalation starts with nucleation of irregular wrinkles near the Na probe. With further sodium intercalation, these wrinkles propagate as the reaction front. In Fig. 2b, the diffusivity is estimated to be ~$0.2–0.9\times10^{-10}$ cm^2/s from the equation $D=d^2/2t$(ref.[14]), where D is diffusivity, t is the diffusion time, and d is the diffusion distance which approximately corresponds to the square root of the sodium intercalation domain area. However, it should be noted that this calculation could only give us an approximate value of the diffusivity, as there are a few variables in practical experiments (e.g., contact condition, bias, and sample size) can influence the estimation. A typical higher magnification of TEM image in Fig. 2c shows that the wrinkled phase boundary zone which separates the pristine SnS_2 domain and sodium intercalated Na_xSnS_2 domain is about 20–50 nm in width. At the zone of phase boundary (Fig. 2d), the presence of dislocations and defects with lattice distortion is confirmed from the Fast Fourier space filtered image in Fig. 2e, suggesting the sodium ion migration causes the fracture of layer structure. Indeed, the Na migration induced structure fracture has also been observed in MoS_2 nanostructures [18].

The sodium insertion reaction in SnS_2 (discharging) is thermodynamically favorable and facile reaction [11]. Whether the sodium ions can be fully extracted (charging) is prerequisite for the rechargeable SIBs. We find that once the reactions are controlled within the range of sodium intercalation, the inserted sodium ions can be completely pulled out. However, during the sodium extraction, instead of simple phase boundary retraction, small domains with superstructure stripes are observed in Fig. 3a. In addition, the nucleation of these domains is inhomogeneously in Fig. S3. These superstructures disappear completely after 166 s, implying the intermediate nature of these superstructures. The lattice fringes in Fig. 3 have been almost fully recovered after sodium extraction, which is of importance to the cycle performance of the electrode. FFT patterns in Fig. 3b further confirm that the superstructures have reflections of {½ 0 0}. In the FFT filtered image in Fig. 4a, the space of the superstructure stripes is measured to be twice of {100} planes. On the basis of the high resolution and FFT patterns, an atomistic structure model is proposed in Fig. 4b. Seen from [001] direction, in every two-unit cell only one is occupied by sodium ions along [110] direction, namely, $Na_{0.5}SnS_2$. An atomistic model seen along [110] is shown in Fig. 4c, where within every (001) Na layers, Na ions occupy every other row. Such structure is further confirmed by the electron diffraction simulation in Fig. 4d–g.

Locally ordered structures were also reported in several lithium compounds such as Li-graphite [28] and TaS_2,(ref. [17]), namely

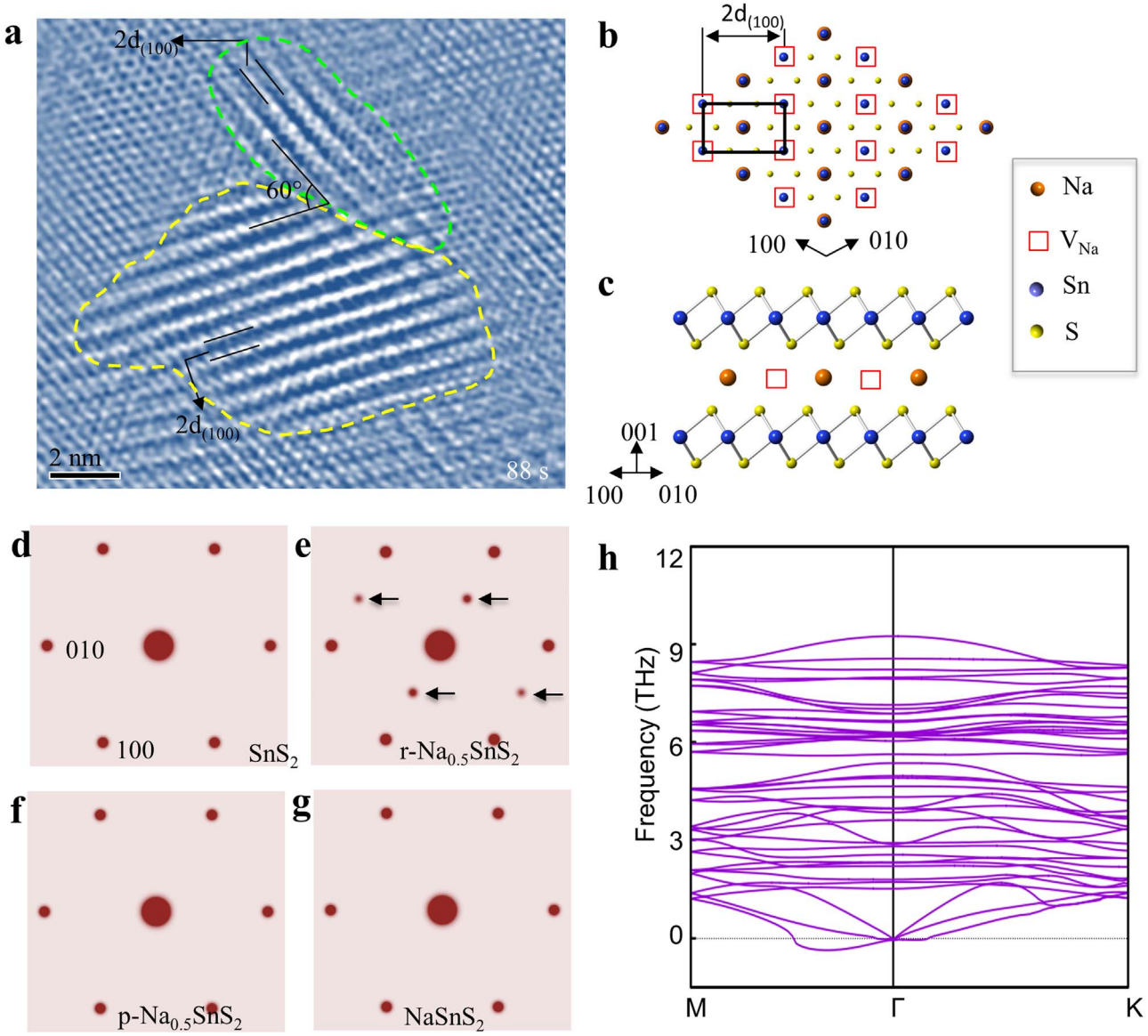

Fig. 4. Sodium ordering phase. (a) FFT filtered image at 88 s. An atomistic structure of the superstructure therefore is proposed with viewing directions of (b) [001] and (c) [110]. Simulated electron diffraction patterns of (d)SnS_2, (e)$Na_{0.5}SnS_2$ with row ordering within (001) planes, (f) $Na_{0.5}SnS_2$ with (001) plane ordering, and (g) $NaSnS_2$. (h) Phonon dispersion of the proposed r-$Na_{0.5}SnS_2$ structure. The details of calculations are included in the Supporting information.

staging phases with (001) plane ordering. Formation of the lithium-staging phases was believed to minimize the repulsive interaction between lithium ions as well as the elastic coherence strain energy [29,30]. Our observation in this study shows a new type of structural ordering, i.e., alternative Na and vacancy row ordering within (001) Na planes (r-$Na_{0.5}SnS_2$), which is distinct from the common staging phase with (001) plane ordering (p-$Na_{0.5}SnS_2$). The electron diffraction simulations in Fig. 4e and f show that these two ordered structures have very different electron diffraction patterns. The FFT pattern in Fig. 3b matches the r-$Na_{0.5}SnS_2$ phase rather than the p-$Na_{0.5}SnS_2$. In transition mental oxide $FePO_4$, staging phase $Li_{0.5}FePO_4$ with plane ordering was also observed [31] and the theoretical calculation [32] indicated that the staging phase $Li_{0.5}FePO_4$ was kinetically controlled while thermodynamically metastable in olive Li_xFePO_4. Since the structural ordering mechanism is likely different between the layered metal dichalcogenides and transition metal oxide [32] due to the different nature of bonding, and it does not have to be same for the lithium and sodium intercalation because their different radius size and mass would make distinct impacts on the elastic strain, the underlying mechanism of the row ordering in our study requires future theoretical calculations. Nevertheless, the structural stability of the proposed r-$Na_{0.5}SnS_2$ structure is tested by density functional theory calculations (DFT). We check the existence of negative-frequencies in phonon dispersion, which is a powerful tool to test the structural stability according to previous studies [33,34]. As shown in Fig. 4h, there are no major negative-frequencies phonon modes, indicating the proposed $Na_{0.5}SnS_2$ structure is stable. The small negative frequencies in acoustic mode is due to numerical error which is common in DFT calculations [33].

Note that although the sodium insertion and extraction in SnS_2 are reversible, the reaction pathways are distinct, i.e., sodium intercalation occurs via two-phase reaction while sodium extraction involves intermediate local structure ordering phase that shows solid solution-like behavior. Similar distinct reaction pathways between discharge and charge are frequently observed in the conversion, alloying and displacement reactions [35–40] because when the temperature is relatively low the phase transition in these electrode materials usually follow the nonequilibrium path and therefore structures convert into the phase which is the most easily kinetically reached instead of the thermodynamic ground state [39]. The kinetic phase sequence, unlike

the thermodynamic phase transition, is not reversible during the alkali ions insertion and extraction. It is well known that the asymmetric reaction pathways in the electrode materials can lead to voltage hysteresis and subsequent low energy efficiency. Since the asymmetric reaction pathways are usually only expected in the conversion, alloying and displacement reactions rather than in the intercalation reactions [41], our observations of asymmetric phase transformations during sodium insertion and extraction in SnS_2, therefore, may help us to elucidate the origin of voltage hysteresis for intercalation reaction in layered metal dichalcogenides.

In addition, such asymmetric sodium insertion and extraction behavior, i.e., two-phase sodium intercalation and solid solution-like de-intercalation, have also been reported in MoS_2 from the X-ray diffraction study [19], although the underlying mechanism and details of intermediate and local structure evolution were missing. Considering the structural similarities in these layered metal dichalcogenides, our observations imply that the local structure ordering during Na extraction may also occur in MoS_2 and other layered metal dichalcogenides. We can also compare the sodium intercalation/extraction with lithium migration in the same SnS_2 in the literature [42]. Due to the larger radius and heavier mass for Na, the kinetics and dynamics between lithiation and sodiation processes are usually significantly different for conversion electrode materials such as FeF_2 [43] and intercalation type electrode materials dominated by ionic bond interactions such as MnO_2 [44]. In contrast, for the layered structures with van der Waals interactions such as MoS_2, it was reported that the lithiation and sodiation behavior shared great similarities [16,18]. The SnS_2 also shows very similar behavior between lithium and sodium migration, e.g. two-phase insertion and solid-solution-like extraction with local structure ordering. Therefore, it is likely the radius and mass of the alkali metal ions play less important roles during migration in these layered structures compared to the conversion and ionic bonded electrode materials probably due to the weaker bonding interaction and relative larger space between layers in the van der Waals materials. Nevertheless, there are still a few differences between lithiation and sodiation reactions for SnS_2. The lithium insertion is more facile and faster than the sodium insertion. A sharp phase boundary between SnS_2 and Li_xSnS_2 domains was observed during lithiation of SnS_2 [42]. The phase boundary during lithiation usually moves too fast to be captured by slow scan CCD in a single frame image in the high-resolution mode. In contrast, in this work a region in the width of tens of nanometers containing high density of dislocations and boundaries exists between the non-reacted SnS_2 and intercalated Na_xSnS_2 domains.

3. Conclusions

In summary, we real-time track the sodium ions insertion and extraction in SnS_2 nanostructures with an atomic-scale spatial resolution. Similar with the lithiation process, asymmetric solid-state phase transformations during sodium insertion and extraction are observed. Sodium insertion in SnS_2 occurs via two-phase reaction and the diffusivity is estimated at the level of about 10^{-11}–10^{-10} cm^2/s. Insertion sodium in SnS_2 causes structure fracture to form high density of dislocations and grain boundaries at the reaction front, which was not observed during lithiation. During sodium extraction, nano-sized and intermediate structural ordering phases ($Na_{0.5}SnS_2$) are observed and the atomic structure has been proposed. Overall, although the kinetic behavior for sodium system is more sluggish than the lithiation, both the sodiation and lithiation of SnS_2 show very similar dynamic behaviors, implying these layered structures with van der Waals interactions can be promising candidates for sodium ion battery electrodes. The intermediate phase with row ordering within every (001) Na planes is distinct from that of the widely accepted staging phase with (001) plane ordering. These observations provide valuable insights into the mechanistic understanding of the underlying solid-state phase transformations during ion migration in these layered metal dichalcogenide electrode materials. In particular, the asymmetric sodium insertion and extraction pathways may provide some insights to elucidate the origins of voltage hysteresis in the electrode. Therefore, our study shed light on the design of SIBs with high rate capability and energy efficiency. In addition, a few interesting phenomena are observed here, e.g., sodium intercalation induced fracture, volume expansion, which require more studies from other approaches such as *ex situ* TEM or *in situ* XRD to clarify their effects on the electrochemical properties (e.g. cycling stability). Furthermore, by improving the *in situ* TEM techniques and conducting the experiments in aberration corrected microscopes, it may be possible to directly determine the atomic arrangements of the phase boundary between Na-rich and Na-poor (e.g., Na ions position, Na occupancy, and defect structure) during electrochemical reactions, which would be very valuable for understanding the relation between structure and properties in the electrode materials.

4. Experimental section

In situ TEM experiments. The SnS_2 nanosheets with layered structure were mechanically peeled off from a single crystal by using a half TEM Cu grid to scratch the surface of SnS_2 crystal. The Cu grid acts as one current collector and SnS_2 is considered to be working electrode. The typical thickness of SnS_2nanosheet varies from a few nanometers to tens of nanometers. Sodium metal (acting as the counter electrode) was coated onto a sharp tungsten probe. All of the components were loaded onto a TEM specimen holder (PicoFemto) integrated with mobile electrical biasing probe in Argon filled glove box and then transferred into the TEM column using Argon filled plastic bag. During transferring the holder into the TEM chamber, the sodium metal was intentionally exposed to air (~2 s) to form a thin passivation layer of NaO_x on the surface that acted as solid-state electrolyte to allow transport of sodium ions [23]. The sodium insertion was initiated by applying a small negative bias between the tungsten probe and the grounded Cu grid, while the sodium extraction was driven by a small positive bias.

Data acquisition and analysis. Both TEM images and electron diffraction patterns (ED) were recorded by a Gatan CCD. The atomistic models were generated by Crystalmaker software. The plots were created by Origin 8.5. The FFT patterns and inverse FFT were calculated by DigitalMicrograph (Gatan) software. The simulation of electron diffraction was carried by commercial software SingleCrystal™ 2.3.3 for Mac system.

For the electrochemical measurements, the electrode was prepared by SnS_2 (80 wt%), carbon black (10 wt%), and polyvinylidene fluoride (PVDF, 10 wt%) in N-methylpyrrolidone (NMP) to form a homogenous slurry. The slurry was then spread onto a copper foil and dried at 100 °C for an overnight in a vacuum oven. Sodium metal and glass fiber were used as the anode and the separator, respectively. 1 M $NaPF_6$ in a mixture of ethylene carbonate (EC), dimethyl carbonate (DMC) was used as the electrolyte. 2032 coin cells were assembled in an argon-filled glove box. The batteries were galvanostatic discharged and charged at current density 100 mA/g on a LAND CT2001A cell test apparatus at room temperature. The weight of our electrode materials is about 2.0 mg/cm^2.

Acknowledgements

This work was supported by the National Key Research and Developement Program of China (2016YFA0300903, 2016YFA0300804), National Natural Science Foundation of China (51502007, 51672007, 51502032), the Recruitment Program for Young Professionals of China, and “2011 Program” Peking-Tsinghua-IOP Collaborative Innovation Center of Quantum Matter.

Appendix A. Supplementary information

Supplementary information associated with this article can be found in the online version at doi:10.1016/j.nanoen.2016.12.051.

References

[1] V. Palomares, P. Serras, I. Villaluenga, K.B. Hueso, J. Carretero-Gonzalez, T. Rojo, Energy Environ. Sci. 5 (2012) 5884.
[2] H. Pan, Y.-S. Hu, L. Chen, Energy Environ. Sci. 6 (2013) 2338.
[3] M.D. Slater, D. Kim, E. Lee, C.S. Johnson, Adv. Funct. Mater. 23 (2013) 947.
[4] B. Dunn, H. Kamath, J.-M. Tarascon, Science 334 (2011) 928.
[5] J.B. Goodenough, Y. Kim, Chem. Mater. 22 (2010) 587.
[6] M.M. Doeff, Y.P. Ma, S.J. Visco, L.C. Dejonghe, J. Electrochem. Soc. 140 (1993) L169.
[7] Y. Liu, B.V. Merinov, W.A. Goddard III, Proc. Natl. Acad. Sci. USA 113 (2016) 3735.
[8] Y.-X. Wang, K.H. Seng, S.-L. Chou, J.-Z. Wang, Z. Guo, D. Wexler, H.-K. Liu, S.-X. Dou, Chem. Commun. 50 (2014) 10730.
[9] L. David, R. Bhandavat, G. Singh, ACS Nano 8 (2014) 1759.
[10] J. Wang, C. Luo, T. Gao, A. Langrock, A.C. Mignerey, C. Wang, Small (2014) 1.
[11] B. Qu, C. Ma, G. Ji, C. Xu, J. Xu, Y.S. Meng, T. Wang, J.Y. Lee, Adv. Mater. 26 (2014) 3854.
[12] M. Wilkening, W. Kuchler, P. Heitjans, Phys. Rev. Lett. 97 (2006) 065901.
[13] M. Wilkening, P. Heitjans, Phys. Rev. B 77 (2008) 024311.
[14] A. Van der Ven, J.C. Thomas, Q. Xu, B. Swoboda, D. Morgan, Phys. Rev. B 78 (2008) 104306.
[15] A. Van der Ven, J. Bhattacharya, A.A. Belak, Acc. Chem. Res. 46 (2013) 1216.
[16] L. Wang, Z. Xu, W. Wang, X. Bai, J. Am. Chem. Soc. 136 (2014) 6693.
[17] H. Fernande, M. Ohstuki, A. Hibino, C. Hough, Science 174 (1971) 498.
[18] P. Gao, L. Wang, Y. Zhang, Y. Huang, K. Liu, ACS Nano 9 (2015) 11296.
[19] X. Wang, X. Shen, Z. Wang, R. Yu, L. Chen, ACS Nano 8 (2014) 11394.
[20] X. Yu, et al., Adv. Energy Mater. 4 (2014) 1300950.
[21] J.Y. Huang, et al., Science 330 (2010) 1515.
[22] J. Niu, A. Kushima, X. Qian, L. Qi, K. Xiang, Y.-M. Chiang, J. Li, Nano Lett. 14 (2014) 4005.
[23] X.H. Liu, et al., Nat. Nanotechnol. 7 (2012) 749.
[24] Y. Zhu, et al., Adv. Mater. 25 (2013) 5461.
[25] M.T. McDowell, Z. Lu, K.J. Koski, J.H. Yu, G. Zheng, Y. Cui, Nano Lett. 15 (2015) 1264.
[26] K. He, et al., Nano Lett. 15 (2015) 1437.
[27] I. Lefebvre-Devos, J. Olivier-Fourcade, J.C. Jumas, P. Lavela, Phys. Rev. B 61 (2000) 3110.
[28] J.E. Fischer, T.E. Thompson, Phys. Today 31 (1978) 36.
[29] S.A. Safran, D.R. Hamann, Phys. Rev. B 22 (1980) 606.
[30] S.A. Safran, D.R. Hamann, Phys. Rev. Lett. 42 (1979) 1410.
[31] L. Gu, C. Zhu, H. Li, Y. Yu, C. Li, S. Tsukimoto, J. Maier, Y. Ikuhara, J. Am. Chem. Soc. 133 (2011) 4661.
[32] Y. Sun, X. Lu, R. Xiao, H. Li, X. Huang, Chem. Mater. 24 (2012) 4693.
[33] S. Cahangirov, M. Topsakal, E. Akturk, H. Sahin, S. Ciraci, Phys. Rev. Lett. 102 (2009) 236804.
[34] Y.Y. Zhang, R. Mishra, T.J. Pennycook, A.Y. Borisevich, S.J. Pennycook, S.T. Pantelides, Adv. Mater. Inter. 2 (2015) 1500344.
[35] U. Boesenberg, M.A. Marcus, A.K. Shukla, T. Yi, E. McDermott, P.F. Teh, M. Srinivasan, A. Moewes, J. Cabana, Sci. Rep. 4 (2014) 7133.
[36] D. Chang, H. Huo, K.E. Johnston, M. Ménétrier, L. Monconduit, C.P. Grey, A. Van der Ven, J. Mater. Chem. A 3 (2015) 18928.
[37] H.C. Yu, C. Ling, J. Bhattacharya, J.C. Thomas, K. Thornton, A. Van der Ven, Energy Environ. Sci. 7 (2014) 1760.
[38] B. Key, M. Morcrette, J.-M. Tarascon, C.P. Grey, J. Am. Chem. Soc. 133 (2011) 503.
[39] R.E. Doe, K.A. Persson, Y.S. Meng, G. Ceder, Chem. Mater. 20 (2008) 5274.
[40] J.K. Ko, K.M. Wiaderek, N. Pereira, T.L. Kinnibrugh, J.R. Kim, P.J. Chupas, K.W. Chapman, G.G. Amatucci, ACS Appl. Mater. Interfaces 6 (2014) 10858.
[41] W. Dreyer, J. Jamnik, C. Guhlke, R. Huth, J. Moskon, M. Gaberscek, Nat. Mater. 9 (2010) 448.
[42] P. Gao, L.P. Wang, Y.Y. Zhang, Y. Huang, L. Liao, P. Sutter, K.H. Liu, D.P. Yu, E.G. Wang, Nano Lett. 16 (2016) 5582.
[43] K. He, et al., ACS Nano 8 (2014) 7251.
[44] Y.F. Yuan, et al., Nano Energy 19 (2016) 382.

Peng Gao is an assistant Professor in School of Physics, Peking University, Beijing, China. He received his Ph.D. degree in condensed mater physics from the Institute of Physics, Chinese Academy of Sciences in 2010. He was a postdoctor in University of Michigan (2010–2013), research associate in Brookhaven National Lab (2013–2014), research fellow and Japan Society for the Promotion of Science (JSPS) foreign fellow in University of Tokyo (2014–2015). He jointed in Peking University in 2015. His research interests include electron microscopy, ferroelectrics, solid-state ionics, and structure and properties of crystal defects and interfaces.

Yu-Yang Zhang is an associate professor in School of Physical Sciences, University of Chinese Academy of Sciences, China. He obtained his Ph.D. degree from Institute of Physics, Chinese Academy of Sciences, China (2012). He took two terms of postdoc in Rensselaer Polytechnic Institute and Vanderbilt University, USA. His research interest is to use quantum-mechanical calculations based on density functional theory (DFT) to understand the fundamental physics in materials and devices for future nano-electronics and energy-related applications.

Liping Wang is an associate professor in University of Electronic Science and Technology of China. She received her PhD degrees (2011) in Institute of Physics, Chinese Academy of Sciences and Laboratoire de réactivitéetchimie des solides, Université de Picardie Jules Verne, France. She worked as a post-doctoral fellow in Max Planck Institute of Colloids and Interfaces, Germany (2012) and Brookhaven National Lab, United States (2013–2014). Her current research interests are structure-property correlations of electrode materials as energy storage devices.

Shulin Chen is a postgraduate student in School of Materials Science, Harbin Institute of Technology. He received his Bachelor's degree from Harbin Institute of Technology at Weihai in 2015. He joined Prof. PengGao's group in February 2016 as a joint PhD candidate. He is especially interested in studying lithium ion batteries by using the electron microscopy techniques.

Yuan Huang is a research associate in Center for Functional Nanomaterials, Brookhaven National Laboratory. He received his Ph.D. degree (2013) in Institute of Physics, Chinese Academy of Sciences, and then he joined Prof. Peter Sutter's group in Brookhaven National Lab. His currently interests are exfoliation of two-dimensional nanomaterials, nano-device fabrication and electrical transport measurements.

Xiumei Ma is an engineer in School of Physics, Peking University. She received her Ph.D. degree (2011) in College of Applied Science, Beijing University of Technology, and then joined Electron Microscopy Laboratory, Peking University. Her current interest is thin film oxide materials.

Kaihui Liu is currently a Professor of Physics, Peking University, Beijing, China. Dr. Kaihui Liu's main research interests are the novel physical phenomena and controllable growth in nanoscale structures, especially in 1D carbon nanotubes and 2D graphene. He developed an advanced single nano-object level in-situ Nano-optics + TEM technique, and in-situ Nano-optics + CVD technique to study structure-dependent physics and growth mechanism at nano scale.

Dapeng Yu is a Chang Kung professorship in Physics in School of Physics, Peking University. He received his PhD. Degree (1993) in Laboratoire de Physicque des Solides, Université Paris-sud, Orsay, France, and then joined Department of Physics, Peking University in 1995. He became a member of Chinese Academy of Sciences in 2015. His current interests are 1-D semiconductor nanowires, transport in low-D materials, and single DNA detection/sequencing via solid statenanopore microscope.